Nanopore Gradients on Porous Aluminum Oxide Generated by Nonuniform Anodization of Aluminum

Krishna Kant,[†] Suet P. Low,[‡] Asif Marshal,[§] Joseph G. Shapter,[§] and Dusan Losic*[,†]

Ian Wark Research Institute and Mawson Institute, University of South Australia, Mawson Lakes Campus, Mawson Lakes, Adelaide, SA 5095, South Australia, Australia, and School of Chemical and Physical Sciences, Flinders University, GPO Box 2010, Adelaide, South Australia, Australia

ABSTRACT A method for surface engineering of structural gradients with nanopore topography using the self-ordering process based on electrochemical anodization of aluminum is described. A distinct anodization condition with an asymmetrically distributed electric field at the electrolyte/aluminum interface is created by nonparallel arrangement between electrodes (tilted by 45°) in an electrochemical cell. The anodic aluminum oxide (AAO) porous surfaces with ordered nanopore structures with gradual and continuous change of pore diameters from 80 to 300 nm across an area of 0.5−1 cm were fabricated by this anodization using two common electrolytes, oxalic acid (0.3 M) and phosphoric acid (0.3 M). The formation of pore gradients of AAO is explained by asymmetric and gradual distribution of the current density and temperature variation generated on the surface of Al during the anodization process. Optical and wetting gradients of prepared pore structures were confirmed by reflective interferometric spectroscopy and contact angle measurements showing the ability of this method to generate porous surfaces with multifunctional gradients (structural, optical, wetting). The study of influence of pore structures on cell growth using the culture of neuroblastoma cells reveals biological relevance of nanopore gradients and the potential to be applied as the platform for spatially controllable cell growth and cell differentiation.

KEYWORDS: structural gradients • pore gradients • optical gradients • nanoporous alumina • anodization • neuroblastoma cells

1. INTRODUCTION

The past two decades have witnessed major advances in developing methods for decorating surfaces of materials with chemical or physical patterns including surface gradients, where physical and chemical properties change continuously along the surface (1). Functional surface gradients in particular have generated great interest for a number of fundamental studies and applications including studies of biomolecular interaction, influence on cell morphology, growth and motility, tissue engineering, diagnostics, nanotribology, drug delivery, microfluidics, and cell biology (2−4). The biological gradients are, for example, the key for many of the physiological and pathological processes but remain poorly understood (4). Thus, there is an acute need to develop biomaterial platforms, to mimic and facilitate the study of biological gradients. Two broad approaches such as bottom-up and top-down were used for the preparation of chemical and structural gradients involving chemical composition, interfacial properties (hydrophobicity/hydrophilicity), morphology, and density (1−5). These gradients were prepared by different techniques and materials using diffusion, self-assembly, plasma discharge, vapor deposition, lithography, and electrochemical methods (1, 2, 4, 6, 7).

Although many structural gradients in the form of nanoparticles, nanowires, nanorods, and surface roughness have been reported, it is surprising that nanopore gradients have not widely been explored (8). Pore structures with nanoscale dimensions exhibit many useful properties for applications in photonics, catalysis, energy storage, molecular separation, biosensing, microfluidcs, cell growth, and drug delivery (9−13). The application of pore gradients is first demonstrated by Sailor's group using electrochemically machined pores in silicon for determining protein size (14). In comparison with electrochemical etching, a self-ordering anodization process is another fabrication approach with capacity to generate nanopore arrays with a superior order of pores and control of pore dimensions (15). Nanoporous anodic aluminum oxide (AAO) and nanotubular titania (TNT) are the most explored examples prepared by this method. Particularly, because of their biocompatibility, they are widely used for study of cell growth and drug delivery (10, 12, 16, 17). Both in vitro and in vivo cell studies on AAO and TNT have demonstrated the influence of pore structures on cell adhesion with a significant increase in growth rate (osteoblast cells) in comparison with a nonporous surface (2, 16, 17). Most significant results recently reported show that the diameter of (TNT) nanopores can control the destiny of human and rat mesenchymal stem cells (MSC) and tune their differentiation into osteoblast cells (18, 19). These studies undoubtedly suggest that nanopore gradients are an attractive approach to mimic biological gradients offering a great

* Corresponding author. E-mail: dusan.losic@unisa.edu.au. Phone: + 61 8302 6862. Fax: +61 8302 3683.
Received for review June 9, 2010 and accepted November 9, 2010
[†] Ian Wark Research Institute, University of South Australia.
[‡] Mawson Institute, University of South Australia.
[§] Flinders University.
DOI: 10.1021/am100502u

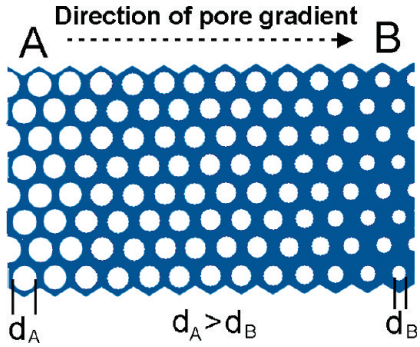

FIGURE 1. Schematic presentation of surface with pore gradients fabricated by self-ordered electrochemical anodization that consists of a continuous change of pore diameters across the surface (A to B).

potential for spatially controllable cell growth, cell implants, and tissue engineering. However, they used the system of a series of individual platforms with distinct pore dimensions which is time-consuming and cost-effective. Hence, the development of single cell platforms with gradual pore topography to screen the best nanoscale architectures for proliferation of a specific cell is an important problem to address.

This work presents a method for engineering surfaces with nanopore gradients on porous AAO that consists of continuous changes of pore diameters across the surface (Figure 1). The method proposes the use of nonlinear or asymmetrical anodization of Al based on spatial distribution of electric filed at the electrode/electrolyte interface. It is well-known that the diameters of AAO pores formed during anodization can be controlled by applied voltage or current (20). This process requires application of a voltage between an Al electrode (anode) and a cathode (Pb, Pt, C) which are in a conventional process arranged in parallel, to make an equally dispersed electric field on the Al surface (21). Hence, to create a spatial and continuous change of pore diameters across AAO, we explored anodization conditions based on an angled arrangement between electrodes to generate a spatial distribution of current density. By this electrode arrangement, the potential at the aluminum/solution interface is expected to be a function of the distance from the cathode due to the resistance of the electrolyte solution, which leads to a decrease in current density as the distance from the electrode increases (14). The changes in current density will ultimately result in a gradient of pore dimensions, which is controllable by applied voltage, current, or selection of electrolytes (e.g., oxalic acid will produce smaller pores with smaller diameter of those produced in phosphoric acid). A similar concept has been successfully used to generate dispersed voltage or current on electrode surface for metal electrodeposition processes (The Hull's cell) and electrochemical etching of silicon (7, 14, 22, 23). This paper presents the application of the method of asymmetrical anodization on Al, to explore its ability to create the porous platform on AAO with continuous pore gradients with a range of pore diameters and distinct nanostructural features. The fabricated nanopore gradients were used to study the influence of pore topography on cell adhesion and morphology using human neuroblastoma cells as a culture cell model.

2. EXPERIMENTAL SECTION

2.1. Materials. High purity Al foil (99.997%, 0.1 mm thickness) supplied by Alfa Aesar (USA) and low purity Al foil (99.6%, 0.050 mm thickness) supplied by Sigma-Aldrich were used as the substrate for fabrication of AAO. Oxalic acid, phosphoric acid, perchloric acid, glutaraldehyde, formaldehyde, ethanol, acetone, and other chemicals were supplied from Sigma-Aldrich (Australia) and Chem-Supply (Australia) and used as received. Human SK-N-SH cells derived from neuroblastoma (neuronal tumor of an embryonic origin) were maintained in DMEM (Dulbecco's modified eagle medium) with 10% (v/v) fetal bovine serum and supplemented with penicillin/streptomycin .

2.2. Preparation of AAO Substrates. Al foils were cleaned by sonication in acetone for a minimum of 1 h prior to the anodization process. Al foil was then electrochemically polished in an 1:4 mixture solution of 65% $HClO_4$ and 99.5% ethanol (5 °C). The electrochemical cleaning is not performed in an anodization experiment using a low purity Al foil to preserve its native surface topography. A mirror finished Al foil after polishing was placed in a custom-made electrochemical cell which allows changing of the angle between the Al (anode) and Pb electrode (cathode). The angled arrangement (45°) between electrodes was applied to achieve nonlinear anodization. A parallel electrode arrangement was used as control. The Al electrode area exposed to the electrolyte solution was 1 × 2 cm, 1 × 3 cm, or 1 × 5 cm. The anodization (hard anodization, HA) process was performed in galvanostatic mode with constant current density of 100−150 mA/cm^2 using a power supply (Agilent, USA) and electrolytes, 0.3 M oxalic acid or 0.3 M phosphoric acid (volume 0.5 L) (24). The voltage during anodization process was self-adjusted by the power supply and not specifically controlled. Both current and voltage signals were recorded by software and a personal computer connected to a power supply (24) (Figure S1, Supporting Information). The temperature in the cell was kept at 0 °C, and the anodization process was performed over 2−5 min to prepare a thinner porous layer and 5−20 min to prepare thicker porous layer. A low stirring condition of electrolyte is applied during anodization. The color change across the Al surface was used as a coarse indication of the pore gradient formation and spatial distribution of current during the anodization process.

2.3. Cell Growth on AAO. Prior to cell culture, the prepared AAO samples were sterilized by soaking in 100% (v/v) ethanol and allowed to dry under sterile air before being placed into 6-well plates. Human neuroblastoma cells, SK-N-SH, were seeded onto the AAO samples at a density of 100 000 cells/well and allowed to incubate overnight at 37 °C. A sterile glass coverslip was used as a positive control surface. After incubation, the samples were gently washed with PBS to remove any nonadherent cells and then fixed with a mixture of 2.5% glutaraldehyde and 4% formaldehyde in phosphate buffer for 10 min. The samples were then washed twice with PBS to remove any traces of fixative. The samples were then dehydrated by sequential immersion in graded ethanol baths, starting at 50%, 70%, and 95% and then two separate 100% (v/v) ethanol baths with a final immersion in xylene.

2.4. Characterization. Structural characterization of prepared AAO pore gradients before and after neuronal cell culture was performed using a field emission scanning electron microscope (SEM; FEI Phenom, Helios). The samples were cut into small pieces, mounted on a holder with double sided conductive tape, and coated with a layer of platinum a few nanometers thick. Images with a range of scan sizes at normal incidence and at a 90 degree angle were acquired from the top and cross sections. Static (sessile drop) water contact angles (CA) were

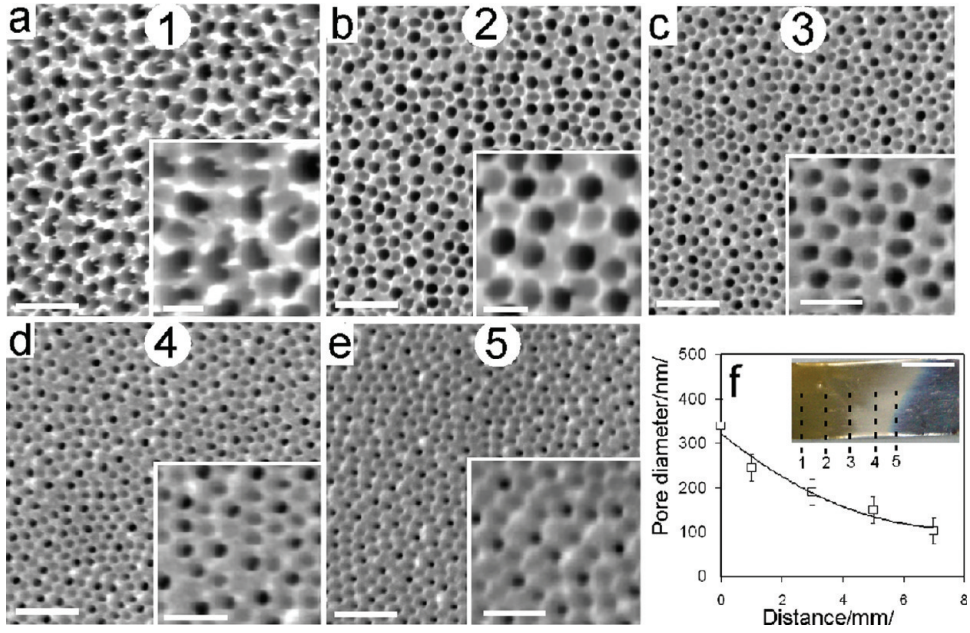

FIGURE 2. (a−e) SEM images of prepared AAO pore gradients showing the pore diameters at different locations formed during anodization. The bar scales are 1 μm and 500 nm (insets). Anodization was performed in 0.3 M oxalic acid with current density of 100 mA/cm^2 at 0 °C, and the angle between electrodes was 45°. (f) Graph showing a gradual change of pore diameters by distance from the front of the electrode. Inset: Photo of AAO with pore gradients with marked locations (1−5) where SEM images were acquired (bar scale is 5 mm).

determined on prepared AAO gradients with a custom-built contact angle goniometer. Reflective interferometric spectroscopy using a fiber optic spectrometer (Ocean Optics JAZEL 200 (USA)) was used to probe their optical properties. A white light from a tungsten lamp was fed through one end of a bifurcated optical fiber at normal incidence on the AAO surface on different spots across the gradient (from 0 to 10 mm). The reflected light from pore surface was collected though the same optical fiber, and reflective interference patterns (Fabry−Perot fringes) were recorded by Ocean Optics Software. A Fourier transform using a multidimensional algorithm from the Wavemetrics Inc. (www.wavemetrics. com) IGOR program library (FFT) was applied. The Fourier transform of the spectrum yields a peak whose position on the *x*-axis corresponds to the value of 2 nL or the effective optical thickness of the porous surface (25).

3. RESULTS AND DISCUSSION

Two anodization conditions were explored in this work using oxalic acid (0.3M) and phosphoric acid (0.3 M), commonly used as electrolytes for preparation of AAO pore gradients (21, 26). The main reason for the use of these two acids instead of sulfuric acid was to achieve gradients with large pore diameters, which can be more easily visualized by SEM. An anodization process was performed using a high current density anodization process (HA) instead of a low current process (mild anodization, MA) because our preliminary results showed that this condition provides a larger change in current density across the electrode surface and, therefore, it is more effective for the formation of pore gradients. Figure 2 shows representative SEM images (Figure 2a−e) of AAO with lateral pore gradients prepared by anodization of Al foil in 0.3 M oxalic acid and acquired from locations at different distances from the edge closest to the cathode. The photo of AAO (Figure 2f, inset) shows a continuous change in color of AAO over an area of 1 cm, from dark yellow to bright yellow. SEM images at different locations show continuous decreasing pore diameters from points 1 to 5. Images acquired at location 1 (Figure 2a), closest to the cathode (Figure 1a,b, spot A), showed the largest pore diameters of typically 305 ± 30 nm. At this location, we expected to have the highest current density (100 mA/cm^2) which corresponds to HA anodization (20, 24). Images of pores (Figure 2e) taken at location 5, the furthest away from the cathode, where we expected to have significantly decreased current density, showed the smallest diameters (130 ± 25 nm). A similar trend was observed for changes in interpore distance from 300 to 250 nm. The graph (Figure 2f) of pore diameters vs distance from the edge (0−10 mm) shows a continuous change of pore diameters and slightly exponential relation with distance. The pore diameter ratio of 2.34 (the largest vs the smallest pores) taken at different distances (d_0/d_8) was determined.

A gradual change in the CA from 105° ± 7° (at location 1) to 65° ± 5° (at location 5) from water droplets on prepared gradients was determined by static CA measurements. This result confirms that the surface with a continuous change of wetting properties can be generated by this method. Fluorescence image from the AAO surface obtained under UV illumination showed a similar trend of continuous decreasing fluorescence intensity across the pore gradients. The result indicates the presence of optical gradients that corresponds to changes of pore structures. To investigate the relation between optical gradients and pore gradients, we performed the thin film interference spectroscopy and acquired reflective interferometric spectra across the gradient surface. Figure 3a shows a light reflectance spectrum taken from several spots from AAO (across 1−5 mm), showing typical patterns (Fabry−Perot fringes) of pore structures. The difference in reflective graphs taken at a different location of gradients (from 5 to 1 mm) is observed including fringeless graph and fringe graphs with different

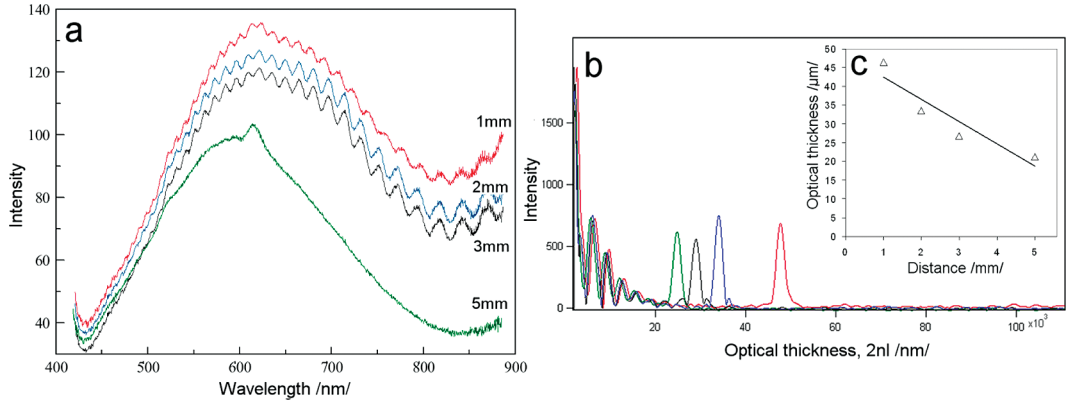

FIGURE 3. Optical characteristics of AAO surface with pore gradients. (a) White light reflectance spectrum taken from several spots from gradients (location 1−5 mm from the edge) showing typical patterns (Fabry−Perot fringes) of pore structures. (b) Fourier transform of the reflectance spectrum in (a) shows a single peak which position along the *x*-axis corresponds to the effective optical thickness of the porous layer (film), 2 nL. (c) The graph of optical thickness versus distance across pore gradients shows a gradual decrease of optical thickness, which corresponds to a decrease of pore thickness and pore diameters.

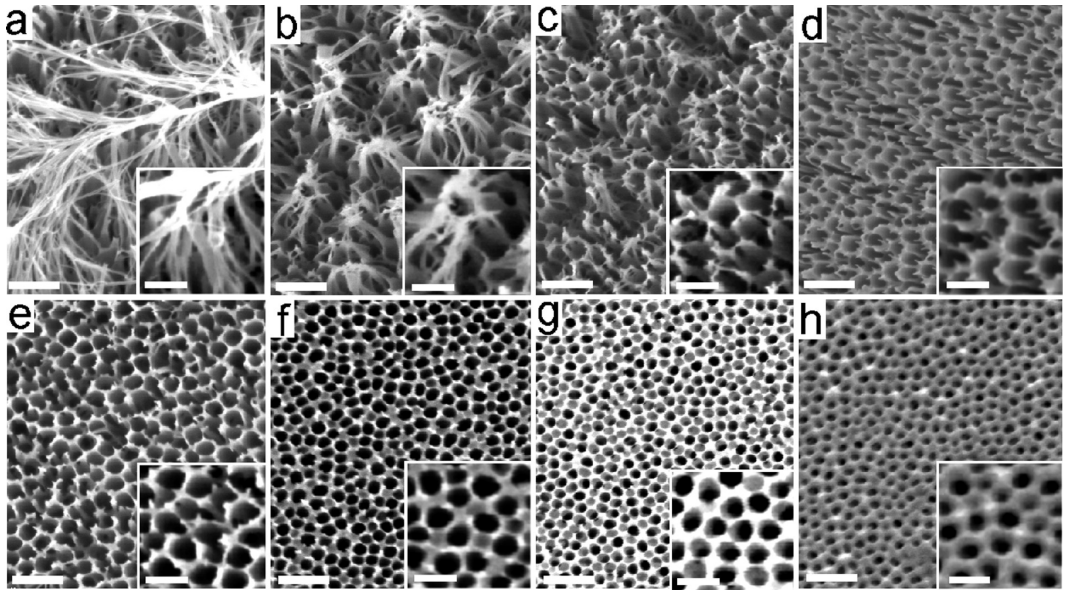

FIGURE 4. (a−h) SEM images of pore gradients with continuous change of pore diameters taken at different locations of AAO. Direction of gradients follows increase in distance between Al electrode and cathode. Anodization was performed in phosphoric acid (0.3 M) with applied current density of 150 mA/cm^2; angle between electrodes was 45°, and the temperature was 0 °C. The bar scales are 1 μm and 500 nm (insets).

numbers of fringes and intensity. The Fourier transform of the reflectance spectra were generated from these graphs as single peaks (Figure 3b) which position corresponds to the effective optical thickness of the porous layer (2 nL). The graph of optical thickness versus distance from the front of AAO is presented in Figure 3c and evidently shows a gradual decrease of optical thickness across the pore gradients. This decrease of optical thickness corresponds to a decrease of the pore thickness and decrease of the pore diameters previously shown in Figure 2f. The results presented here illustrate the impact of pore structures on their optical and wetting properties, confirming that this method can be used to create surfaces with multifunctional gradients which includes continues change structural (pores), optical (interference, fluorescence), and wetting (CA) properties.

Figure 4 summarizes SEM images of AAO pore gradients prepared using phosphoric acid as electrolyte. Images are taken at different locations from the front edge across the length of 5−7 mm and show more dramatic structural pore changes in comparison with the previous example using oxalic acid (Figure 2). Characteristic brushlike structures with pores were observed at the point closest to the cathode (Figure 4a), where we expected to have the highest anodization current (150 mA/cm^2). These brushes are remnants of the pore walls, formed as result of dissolution of the barrier oxide layer between the pores. The formation of brushlike or nanotiplike structures was reported by others using anodization conditions with a high current density (HA) where extensive dissolution of oxide layer has occurred as a result of locally increased temperature or by the use of the chemical etching (dissolution) of the porous layer in phosphoric acid (10%) after the anodization process (27, 28) SEM images (Figure 4a−c) show a continuous change of morphology of brush structures as the distance between electrodes increased, which include gradual decreasing of brush length from a large (partially collapsed) structure with

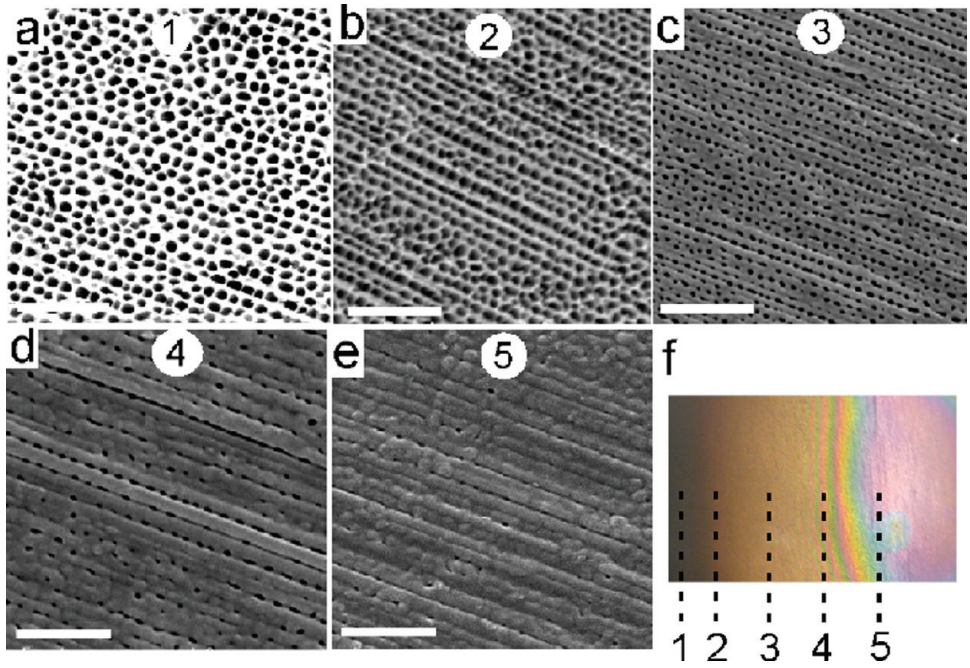

FIGURE 5. (a−e) SEM images of prepared pore gradient surface showing different pore diameters at different locations on the angled electrode formed during anodization of low purity Al foil. The anodization was performed in 0.3 M phosphoric acid with applied current density of 100 mA/cm^2; the angle between electrodes was 45°, and the temperature was 0 °C. The bar scale is 1 μm. (f) Photo of prepared AAO pore gradient surface with marked locations (1−5) where SEM images were acquired. The bar scale is 5 mm.

length >1 μm (Figure 4a), to shorter (<1 μm) and less collapsed structures (Figure 4b), to a very short nanotip structure (Figure 4c), and finally to pores with minor or no brush structure (Figure 4d−f). Presumably, these gradual changes are a result of lateral decreasing of current density across the surface, leading to a decrease in oxide layer dissolution. Finally, at locations on the electrode furthest away from the cathode, brush structures were no longer present, and only changes in pore diameters (from 345 ± 35 nm to 195 ± 20 nm) were observed (Figure 4f−h).

In the case when the aluminum surface is pretextured, this approach can be used to prepare even more complex topography with pore gradients. Figure 5a−e shows one example of topography of pore gradients with pores aligned in parallel lines, prepared by the first anodization in phosphoric acid using a low purity Al foils (96.5%). These rows were generated from structural features of an Al surface inherited from Al foil production, and electropolishing was not used for their removal. The photo (Figure 5f) shows gradual changes of color from golden to pink, corresponding to the gradual changes of pore dimensions and thickness of the porous layer. The locations with darker color and largest pore diameters (110 ± 10 nm), marked as 1 and 2 correspond to the shortest distance between the electrodes and were exposed to the higher current, and locations marked as 4 and 5 were a greater distance from the cathode and had smaller pore diameters (40−50 nm; Figure 5f). The optical properties of the porous layer were gradually changed following changes of pore structures confirming that this method can be used to prepare surfaces with an optical gradient.

Although we could not directly measure the current distribution at different locations on the Al electrode during anodization, the morphology of pore structures and color of prepared AAO indicates that pore gradients were produced by the gradual change of current density on the electrode surface. Our results showed that the largest pores prepared by anodization in oxalic and phosphoric acid (Figures 2a and 4a,b) were formed at locations closest between the electrodes, where a higher current is expected until the smallest pores were observed at locations with a larger distance between electrodes as result of an anodization process with declined current density. To confirm this statement, we performed a series of anodization experiments using different current densities from 140 to 2 mA/cm^2 with a parallel arrangement between electrodes. Photos and SEM images of prepared porous substrates presented in Figure S2 (Supporting Information) clearly show that the gradual change of pore structures are results of the gradual change of current across the Al surface. These results are in agreement with previous studies on electrochemical metal deposition using a similar arrangement between electrodes (Hull's cell) where exponential distribution of current density was measured and modeled (22, 29).

The formation of pore gradients with structural features such as brushes and tips at locations where a higher current density is applied indicates that a locally increased temperature also plays a significant role during the pore formation process. It is well documented that the electrolyte temperature and the hydrodynamics conditions in the electrolytic cell affects the pore diameter (30, 31). Anodic oxidation is an exothermic process, and as a result of the increasing local temperature during pore formation, a chemical dissolution of oxide in the inner layer, as well as the electrochemical formation of anodic oxide layer, is expected to be accelerated (32). This phenomenon is exactly what is observed in

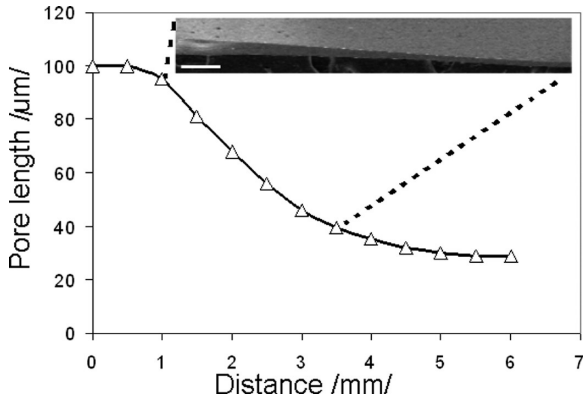

FIGURE 6. Cross-sectional SEM image of AAO with pore gradients (conditions as in Figure 4 but with longer anodization time to obtain thicker layer, followed by removing underlying Al) and the graph showing changes of the pore length (thickness) across the AAO. The bar scale is 200 μm.

our experiment (Figure 4a–c) with the formation of brushed nanostructures as result of an extensive temperature promoted dissolution process of an outer oxide layer in electrolyte (phosphoric acid). The oxide dissolution process when oxalic acid is used as electrolyte is considerably slower which explains the absence of brushed nanostructures during anodization in oxalic acid (Figure 2).

Reflective interference results show that the optical thickness of a porous layer of prepared gradients is gradually decreasing which indicate the difference on pore growth rate across the surface (Figure 3). In order to obtain more information regarding the pore growth process under applied anodization conditions, the cross-sectional SEM image of AAO porous layer with pore gradients was acquired after removing underlying Al. Figure 6 confirms that a gradual change of the thickness of the porous layer of AAO with pore gradients follows the similar trend as pore diameters. The thickness of porous layer or the pore lengths is determined by the growth rate which is proportional to the current density. This result supports our conclusion that the combined effects of the gradual current increase with heat diffusion and nouniform local temperatures on the surface of anodizing aluminum caused by nonparallel electrode arrangement are two main factors that govern the formation of pore gradients. Because this process is based on HA anodization, which is known as a difficult method to obtain self-ordered structures, the influence of a number of other parameters such as anodization mode, type of electrolyte, concentration of electrolyte, purity and roughness of Al electrode, and hydrodynamic condition during the anodization process (e.g., stirring of electrolyte solution) should be considered (20, 21, 26). It is essential to optimize these anodization conditions to maintain a stable self-ordering process and avoid the extensive heat development and the burning effect.

Two main disadvantages of the described anodization process were identified: one is the limitation to extend the lateral length of pore gradients to greater than 10 mm, and the second is an impact of hydrodynamic conditions (stirring solution) on the fabrication reproducibility. It was found that changes in stirring condition (unstirred, low stirring, and high

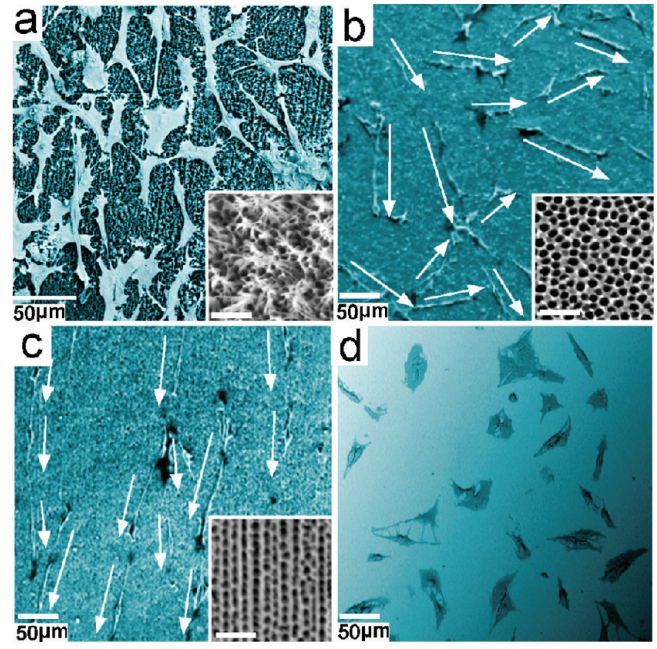

FIGURE 7. Morphological changes of neuroblastoma cells grown on different pore structures of AAO. (a) Polygonal morphology of cells on pores with nanobrushes showing random oriented cells with the extensive cell to cell interconnection. Inset shows underlying surface with partially collapsed brushes. (b) Elevated linear morphology of cells with random cell orientation on pore structures. Inset shows underlying surface with pores (bar scale, 1 μm). (c) Elevated linear morphology of cells with orientation on which follows orientation of pore structures (lines). Inset shows underlying surface with aligned pores. (d) Polygonal morphology of cells with random orientation grown on control sample (glass).

stirring) have an impact on the lateral dimension of pore gradients and pore diameters. A similar problem is noted in common anodization processes with parallel electrodes where random nonuniformity of pore diameters was observed as result of stirring effect (33). This is evidence that the temperature and the creation of spontaneous temperature gradients during the anodization process is an important factor which influences the dissolution process of the oxide layer and pore diameters. More studies are needed to address these issues in order to optimize and control the gradual anodization process of AAO for reproducible preparation of pore gradients over a large area.

To investigate the influence of the various pore structures on cell attachment, cells were cultured on AAO for 24 h and their morphology on each surface was observed through the use of SEM. We used human neuroblastoma, SK-N-SH cells as our neuronal model. Cells cultured on glass coverslips were used to demonstrate the cells' typical polygonal morphology. Neuroblastoma cell lines have been utilized in the past as a model for the observation of cellular alignment, polarization, and neuronal outgrowth on patterned surfaces (34–37). Our results showed that AAO favored the formation of three different cell phenotypes which are summarized in Figures 7 and 8. The most extensive cell response was found on the surfaces with mixed pore and brush structures (Figures 7a and 8a–b). This surface showed the highest cell attachment where the cells exhibited some neuritelike phenotype with cytoplasmic processes and the most exten-

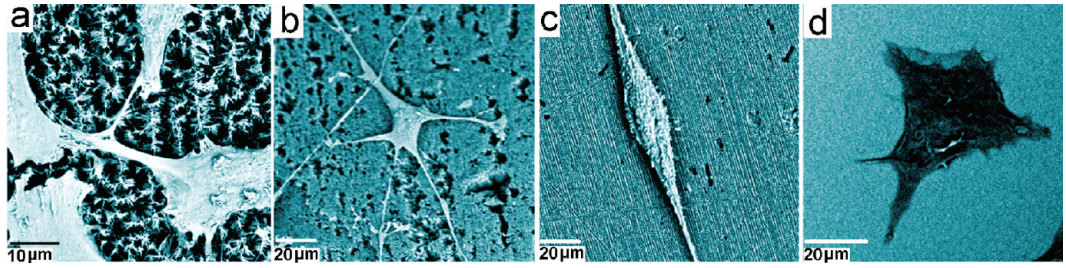

FIGURE 8. SEM images of single neuroblastoma cells grown on different pore structures of AAO. (a,b) Pores with nanobrushes show an extensive branching and interconnection of cells. (c) Aligned pores show a linear morphology of neuroblastoma cell directed by aligned pore structures. (d) Typical polygonal morphology of a cell on a glass surface.

sive cell−cell interactions. The high number of adhered cells indicates that this type of surface topography is conducive to cell attachment and growth. The cells were randomly dispersed, and each cell was interconnected with neighboring cells forming the network (Figure 8a). Cells cultured on pores without brushes and tips structures (Figures 7b−c and 8c) had a more neuritelike phenotype with long bipolar cytoplasmic processes, similar to the axon and dendrite emerging from opposite ends of a neuronal cell. Interestingly, these cells had their neuritelike processes that aligned with the direction of the pore structures.

On AAO with a hexagonal pore organization, the cells were randomly orientated (Figures 7b and S3, Supporting Information), whereas on AAO with a linear pore organization, the cells were aligned with the pore direction (Figures 7c, 8c, and S3, Supporting Information). This demonstrated that pore organization could have a direct influence on the orientation of neuronal cells, opening up bioengineering possibilities. On the control surface, the cells maintained a neuroblast/polygonal morphology with only a few cells exhibiting cytoplasmic processes. The cells on the control surface were also more flattened, indicating strong attachment to the glass surface (Figures 7d and 8d). In comparison, cells on AAO were elevated from the surface attributed to the rough topography, allowing for fewer cell adhesion points. The observation that neuroblastoma cells were able to be aligned to topographical cues on aligned nanopore structures of AAO is an exciting discovery (Figures 8c and S4, Supporting Information). The orientation of nerve cells is critical in nerve regeneration, where cell polarization and axonal outgrowth to form cell−cell interactions are important in maintaining nerve function. The tunability of porous alumina allows for directed cell growth. The open pore structure of AAO can be loaded with chemical moieties, thus the possibility of both topographical and chemical-directed cell growth and migration. This opens up the scope for further investigation of the influence of nanopore structures on the morphology of neuronal cells where we are looking to include surface chemistry as another parameter.

4. CONCLUSION

The fabrication of porous anodic aluminum oxide (AAO) with nanopore gradients which consists of a spatial distribution of pore diameters using a nonuniform anodization process is demonstrated. An anodization approach which allows a spatially asymmetrical anodization was introduced on the basis of creation of an asymmetrical electrical field unparallel arrangement (45°) between electrodes. The method is successfully demonstrated for preparation pore gradients on AAO using two common electrolytes, oxalic and phosphoric acid. In addition to structural gradient, prepared pore structures appear to have optical and wetting gradients confirmed by reflective interferometric spectroscopy and contact angle measurements. Therefore, it is possible to design a surface with multifunctional gradients (structural, optical, wetting) with this method, which are important for application in microfluidics, diagnostics, drug delivery, and cell manipulation. We used the pore gradient surface and neuroblastoma cell to show their potential for pore topography directed cell growth and validate their biological relevance. Pore gradients fabricated by this method open opportunities to design cell culture platforms with desired structural, chemical, and growth factor for controlled cell growth and differentiation. It is expected that this method is generic and can be applied for preparation of nanopore and nanotube gradients from other biocompatible metals such as Ti, Ta, and Hf.

Acknowledgment. The financial support of the Australian Research Council (DP 0770930) and the University of South Australia for this work is greatly acknowledged. Authors thank Tushar Kummeria from UniSA for his help during interferometric measurements and Michael J. Sailor from UCSD, USA, for providing his support.

Supporting Information Available: Typical current and voltage graph recorded during anodization process, SEM images of AAO prepared by anodization of low purity Al foil with parallel orientation of electrodes using different current densities, SEM images of polygonal morphology of neuroblastoma cells grown on nanopore gradients nanobrushes, and SEM images of neuroblastoma cells grown on nanopore gradients with aligned pores. This material is available free of charge via the Internet at http://pubs.acs.org.

REFERENCES AND NOTES

(1) Genzer, J.; Bhat, R. R. *Langmuir* **2008**, *24*, 2294–2317.
(2) Morgenthaler, S.; Zink, C.; Spencer, N. D. *Soft Matter* **2008**, *4*, 419–434.
(3) Fok, S.; Domachuk, P.; Rosengarten, G.; Krause, N.; Braet, F.; Eggleton, B. J.; Soon, L. L. *Biophys. J.* **2008**, *95*, 1523–1530.
(4) Vasilev, K.; Mierczynska, A.; Hook, A. L.; Chan, J.; Voelcker, N. H.; Short, R. D. *Biomaterials* **2009**, *31*, 392–397.
(5) Meyyappan, S.; Shadnam, M. R.; Amirfazli, A. *Langmuir* **2008**, *24*, 2892–2899.

(6) Geissler, M.; Chalsani, P.; Cameron, N. S.; Veres, T. *Small* **2006**, *2*, 760–765.
(7) Bohn, P. W. *Annu. Rev. Anal. Chem.* **2009**, *2*, 279–296.
(8) Khung, Y. L.; Barritt, G.; Voelcker, N. H. *Exp. Cell Res.* **2008**, *314*, 789–800.
(9) Davis, M. E. *Nature* **2002**, *417*, 813–821.
(10) Losic, D.; Simovic, S. *Expert Opin. Drug Delivery* **2009**, *6*, 1363–1381.
(11) Takmakov, P.; Vlassiouk, I.; Smirnov, S. *Anal. Bioanal. Chem.* **2006**, *385*, 954–958.
(12) Popat, K. C.; Mor, G.; Grimes, C. A.; Desai, T. A. *Langmuir* **2004**, *20*, 8035–8041.
(13) Velleman, L.; Triani, G.; Evans, P. J.; Shapter, J. G.; Losic, D. *Microporous Mesoporous Mater.* **2009**, *126*, 87–94.
(14) Collins, B. E.; Dancil, K.-P. S.; Abbi, G.; Sailor, M. J. *Adv. Funct. Mater.* **2002**, *12*, 187–191.
(15) Ghicov, A.; Schmuki, P. *Chem.Commun.* **2009**, 2791–2808.
(16) Popat, K. C.; Swan, E. E. L.; Mukhatyar, V.; Chatvanichkul, K. I.; Mor, G. K.; Grimes, C. A.; Desai, T. A. *Biomaterials* **2005**, *26*, 4516–4522.
(17) Losic, D.; Cole, M. A.; Dollmann, B.; Vasilev, K.; Griesser, H. J. *Nanotechnology* **2008**, *19*, 245704.
(18) Oh, S.; Brammer, K. S.; Li, Y. S. J.; Teng, D.; Engler, A. J.; Chien, S.; Jin, S. *Proc. Natl. Acad. Sci. U.S.A.* **2009**, *106*, 2130–2135.
(19) Park, J.; Bauer, S.; Schmuki, P.; von der Mark, K. *Nano Lett.* **2009**, *9*, 3157–3164.
(20) Lee, W.; Ji, R.; Gosele, U.; Nielsch, K. *Nat. Mater.* **2006**, *5*, 741–747.
(21) Thompson, G. E. *Thin Solid Films* **1997**, *297*, 192–201.
(22) Hull, R. O. *J. Am. Electroplat. Soc.* **1939**, *27*, 52–60.
(23) Hossain, S. M.; J Das, J.; Chakraborty, S.; Dutta, S. K.; H Saha, H. *Semicond. Sci. Technol.* **2002**, *17*, 55–59.
(24) Losic, D.; Lillo, M. *Small* **2009**, *5*, 1392–1397.
(25) Alvarez, S. D.; Li, C.-P.; Chiang, C. E.; Schuller, I. K.; Sailor, M. J. *ACS Nano* **2009**, *10*, 3301–3307.
(26) Thompson, G. E. *Thin Solid Films* **1997**, *297*, 192–201.
(27) Sun, Q. W.; Ding, G. Q.; Li, Y. B.; Zheng, M. J.; Shen, W. Z. *Nanotechnology* **2007**, *18*, 215304.
(28) Losic, D.; Losic, D., Jr. *Langmuir* **2009**, *25*, 5426–5431.
(29) McColm, T. D.; Evans, J. W. *J. Appl. Electrochem.* **2001**, *31*, 411–419.
(30) Aerts, T.; Dimogerontakis, T.; De Graeve, I.; Fransaer, J.; Terryn, H. *Surf. Coat. Technol.* **2007**, *201*, 7310–7317.
(31) Vrublevsky, I.; Parkoun, V.; Schreckenbach, J. *Appl. Surf. Sci.* **2005**, *242*, 333–338.
(32) Brevnov, D. A.; Rao, G. V. R.; Lopez, G. P.; Atanassov, P. B. *Electrochim. Acta* **2004**, *49*, 2487–2494.
(33) Schneider, J. J.; Engstler, N.; Budna, K. P.; Teichert, C.; Franzka, S. *Eur. J. Inorg. Chem.* **2005**, 2352–2359.
(34) Ono, S.; Saito, M.; Ishiguro, M.; Asoh, H. *J. Electrochem. Soc.* **2004**, *151*, B473–B478.
(35) Yang, I. H.; Co, C. C.; Ho, C. C. *Biomaterials* **2005**, *26*, 6599–6609.
(36) Johansson, F.; Kanje, M.; Eriksson, C.; Wallman, L. *Phys. Status Solidi C* **2005**, *2*, 3258–3262.
(37) Matsuzawa, M.; Krauthamer, V.; Potember, R. S. *Biosystems* **1995**, *35*, 199–202.

AM100502U